Module 4- Maxwell's Equations in Cylindrical Coordinates

Dr. Masud Mansuripur

Chair of Optical Data Storage, University of Arizona

Dr. Masud Mansuripur is the Chair of Optical Data Storage and Professor of Optical Sciences in the University of Arizona. His areas of research include optical data storage; magneto-optics; optics of polarized light in systems of high numerical aperture; magnetic and magneto-optical properties of thin solid films; magnetization dynamics, integrated optics for optical heads (data storage systems); information theory, optical signal processing, biological data storage, erbium-doped fiber amplifiers and lasers.

Email: masud@u.arizona.edu

Introduction

In many systems of practical interest, electromagnetic waves propagate within linear, isotropic, homogeneous, circularly symmetric media. Examples include hollow-tube microwave wave-guides, optical fibers, fiber lasers, nano-wires, and nano-rods. In this chapter we discuss the solution of Maxwell's equations for systems that exhibit circular symmetry around a given axis. We then proceed to examine the fundamental characteristics of these solutions, which are generally referred to as the modes (or eigenmodes) of the system.

4.1 Solving Maxwell's equations in linear, isotropic, homogeneous, circularly symmetric media

An electromagnetic wave in a system with cylindrical symmetry has eigen functions of the form $\boldsymbol{E}(r,\phi,z,t) = [E_r(r)\hat{\boldsymbol{r}} + E_\phi(r)\hat{\boldsymbol{\phi}} + E_z(r)\hat{\boldsymbol{z}}]\exp(\mathrm{i}m\phi)\exp(\mathrm{i}k_o\sigma_z z)\exp(-\mathrm{i}\omega t)$, with a similar expression for the magnetic field $\boldsymbol{H}(r,\phi,z,t)$. Here $k_o = \omega/c = 2\pi/\lambda_o$, where λ_o is the vacuum wavelength; the integer m is the ~~azim~~uthal mode number; and the complex-~~valued~~ σ_z is the propagation constant along the z-axis. In general, the beam resides within an environment having complex permittivity and permeability $\varepsilon_o\varepsilon(\omega)$ and $\mu_o\mu(\omega)$. As usual, the speed of light in vacuum $c = 1/\sqrt{\mu_o\varepsilon_o}$ and the impedance of free space $Z_o = \sqrt{\mu_o/\varepsilon_o}$. In the absence of free charges and free currents, Maxwell's equations are written

$$E_r + r\partial E_r/\partial r + \mathrm{i}mE_\phi + \mathrm{i}k_o r\sigma_z E_z = 0, \qquad \textit{(Equation 4.1)}$$

$$\varepsilon E_r = \sigma_z Z_o H_\phi - (mZ_o/k_o r)H_z, \qquad \textit{(Equation 4.2a)}$$

$$\varepsilon E_\phi = -\sigma_z Z_o H_r - (\mathrm{i}Z_o/k_o)\partial H_z/\partial r, \qquad \textit{(Equation 4.2b)}$$

$$\varepsilon E_z = (mZ_o/k_o r)H_r + (\mathrm{i}Z_o/k_o r)H_\phi + (\mathrm{i}Z_o/k_o)\partial H_\phi/\partial r, \qquad \textit{(Equation 4.2c)}$$

$$\mu Z_o H_r = (m/k_o r)E_z - \sigma_z E_\phi, \qquad \textit{(Equation 4.3a)}$$

$$\mu Z_o H_\phi = \sigma_z E_r + (\mathrm{i}/k_o)\partial E_z/\partial r, \qquad \textit{(Equation 4.3b)}$$

$$\mu Z_o H_z = -(m/k_o r)E_r - (\mathrm{i}/k_o r)E_\phi - (\mathrm{i}/k_o)\partial E_\phi/\partial r, \qquad \textit{(Equation 4.3c)}$$

$$H_r + r\partial H_r/\partial r + \mathrm{i}mH_\phi + \mathrm{i}k_o r\sigma_z H_z = 0. \qquad \textit{(Equation 4.4)}$$

Substituting for E_r and E_ϕ from ***Equation 4.2a*** and ***Equation 4.2b*** into ***Equation 4.3a*** and ***Equation 4.3b*** yields

$$(\mu\varepsilon - \sigma_z^2)H_r = (m\varepsilon/Z_o k_o r)E_z + \mathrm{i}(\sigma_z/k_o)\partial H_z/\partial r, \qquad \textit{(Equation 4.5)}$$

$$(\mu\varepsilon - \sigma_z^2)H_\phi = -(m\sigma_z/k_o r)H_z + \mathrm{i}(\varepsilon/k_o Z_o)\partial E_z/\partial r. \qquad \textit{(Equation 4.6)}$$

Placing the above expressions for H_r and H_ϕ in Eq.(2c) results in the following 2nd order differential equation for E_z:

$$\partial^2 E_z/\partial r^2 + (1/r)\partial E_z/\partial r + [k_o^2(\mu\varepsilon - \sigma_z^2) - (m/r)^2]E_z = 0. \qquad \textit{(Equation 4.7)}$$

We define the radial propagation constant $\sigma_r = \sqrt{\mu\varepsilon - \sigma_z^2}$, so that the radial coordinate r may be written in normalized form as $\rho = k_o\sigma_r r$. [For given values of μ, ε, and σ_z, we shall always choose the value of σ_r such that $\mathrm{Im}(\sigma_r) \geq 0$.] ***Equation (4.7)*** may now be written as follows:

$$\partial^2 E_z/\partial\rho^2 + (1/\rho)\partial E_z/\partial\rho + (1 - m^2/\rho^2)E_z = 0. \qquad \textit{(Equation 4.8)}$$

In similar fashion, we substitute for H_r and H_ϕ from ***(Equation 4.3a)*** and ***(Equation 4.3b)*** into ***(Equation 4.2a)*** and ***(Equation 4.2b)*** to obtain

$$(\mu\varepsilon - \sigma_z^2)E_r = \mathrm{i}(\sigma_z/k_o)\partial E_z/\partial r - (m\mu Z_o/k_o r)H_z, \qquad \textit{(Equation 4.9)}$$

$$(\mu\varepsilon - \sigma_z^2)E_\phi = -(m\sigma_z/k_o r)E_z - \mathrm{i}(\mu Z_o/k_o)\partial H_z/\partial r. \qquad \textit{(Equation 4.10)}$$

Placing the above expressions for E_r and E_ϕ in Eq.(3c) results in the following 2nd order differential equation for H_z:

$$\partial^2 H_z/\partial r^2 + (1/r)\partial H_z/\partial r + [k_o^2(\mu\varepsilon - \sigma_z^2) - (m/r)^2]H_z = 0. \qquad \textit{(Equation 4.11)}$$

Once again, use of the normalized radial coordinate $\rho = k_o\sigma_r r$ leads to the standard Bessel equation for $H_z(\rho)$, that is,

$$\partial^2 H_z/\partial\rho^2 + (1/\rho)\partial H_z/\partial\rho + (1 - m^2/\rho^2)H_z = 0. \qquad \textit{(Equation 4.12)}$$

The authors would like to acknowledge support from the National Science Foundation through CIAN NSF ERC under grant #EEC-0812072.

We mention in passing that *(Equation 4.12)* could also have been obtained by substituting H_r and H_ϕ of *(Equation 4.5)* and *(Equation 4.6)* into *(Equation 4.4)*. Similarly, *(Equation 4.8)* could have been obtained by substituting E_r and E_ϕ of *(Equation 4.9)* and *(Equation 4.10)* into *(Equation 4.1)*. This should not be surprising, considering that Maxwell's equations are interdependent.

The solutions of *(Equation 4.8)* and *(Equation 4.12)* may now be expressed in terms of Bessel functions of the radial distance r from the z-axis. In general, any linear combination of Bessel functions of the first and second kind, order m, namely, $J_m(\rho)$ and $Y_m(\rho)$, satisfies the above equations. Thus the general form of the cylinder function appearing in the solution to *(Equation 4.8)* and *(Equation 4.12)* will be $\mathcal{C}_m(\rho) = A J_m(\rho) + B Y_m(\rho)$, where A and B are arbitrary complex constants. The derivative of the cylinder function with respect to its complex argument ρ, denoted by $\mathcal{C}'_m(\rho)$, will appear in the expressions for H_r, H_ϕ, E_r, and E_ϕ, as can be readily observed by examining *Equation (4.5), (4.6), (4.9),* and *(4.10).* The following identities will be useful:

$$\rho^2 \mathcal{C}''_m(\rho) + \rho \mathcal{C}'_m(\rho) + (\rho^2 - m^2)\mathcal{C}_m(\rho) = 0, \qquad \textit{(Equation 4.13a)}$$

$$\mathcal{C}_m(\rho) = (\rho/2m)[\mathcal{C}_{m-1}(\rho) + \mathcal{C}_{m+1}(\rho)], \qquad \textit{(Equation 4.13b)}$$

$$\mathcal{C}'_m(\rho) = \mathcal{C}_{m-1}(\rho) - (m/\rho)\mathcal{C}_m(\rho), \qquad \textit{(Equation 4.13c)}$$

$$\mathcal{C}'_m(\rho) = (m/\rho)\mathcal{C}_m(\rho) - \mathcal{C}_{m+1}(\rho), \qquad \textit{(Equation 4.13d)}$$

$$\mathcal{C}_{-m}(\rho) = (-1)^m \mathcal{C}_m(\rho), \qquad \textit{(Equation 4.13e)}$$

$$\mathcal{C}'_{-m}(\rho) = (-1)^m \mathcal{C}'_m(\rho). \qquad \textit{(Equation 4.13f)}$$

We divide the solutions to *(Equation 4.1-4.4)* into two sets; for one set, we let $E_z = 0$, in which case the solution will be referred to as Transverse Electric (TE); for the other, we let $H_z = 0$, and call the solution Transverse Magnetic (TM). Occasionally, it will be possible to express the complete solution to a given problem in terms of either TE or TM modes; this occurs, for instance, when $\sigma_z = 0$ or when $m = 0$. Often, however, the boundary conditions cannot be matched with just one set of solutions; in such cases both TE and TM modes appear in the solution to Maxwell's equations, and the resulting mode will be referred to as EH or HE, depending on whether E_z or H_z dominates the longitudinal field component. The TE mode wavefunctions are written below:

$$\text{TE:}\boldsymbol{E}_m(r) = -(m\mu/k_o r\sigma_r^2)\mathcal{C}_m(k_o\sigma_r r)\hat{\boldsymbol{r}} - (\mathrm{i}\mu/\sigma_r)\mathcal{C}'_m(k_o\sigma_r r)\hat{\boldsymbol{\phi}}, \qquad \textit{(Equation 4.14a)}$$

$$Z_o\boldsymbol{H}_m(r) = (\mathrm{i}\sigma_z/\sigma_r)\mathcal{C}'_m(k_o\sigma_r r)\hat{\boldsymbol{r}} - (m\sigma_z/k_o r\sigma_r^2)\mathcal{C}_m(k_o\sigma_r r)\hat{\boldsymbol{\phi}} + \mathcal{C}_m(k_o\sigma_r r)\hat{\boldsymbol{z}}. \qquad \textit{(Equation 4.14b)}$$

Similarly, the TM mode wavefunctions are given by:

$$\text{TM:}\quad \boldsymbol{E}_m(r) = (\mathrm{i}\sigma_z/\sigma_r)\mathcal{C}'_m(k_o\sigma_r r)\hat{\boldsymbol{r}} - (m\sigma_z/k_o r\sigma_r^2)\mathcal{C}_m(k_o\sigma_r r)\hat{\boldsymbol{\phi}} + \mathcal{C}_m(k_o\sigma_r r)\hat{\boldsymbol{z}}, \qquad \textit{(Equation 4.15a)}$$

$$Z_o\boldsymbol{H}_m(r) = (m\varepsilon/k_o r\sigma_r^2)\mathcal{C}_m(k_o\sigma_r r)\hat{\boldsymbol{r}} + (\mathrm{i}\varepsilon/\sigma_r)\mathcal{C}'_m(k_o\sigma_r r)\hat{\boldsymbol{\phi}}. \qquad \textit{(Equation 4.15b)}$$

The authors would like to acknowledge support from the National Science Foundation through CIAN NSF ERC under grant #EEC-0812072.

The case of $m = 0$ may be simplified as follows:

TE ($m=0$): $\boldsymbol{E}_0(r,\phi,z) = (\mathrm{i}\mu/\sigma_r)\mathcal{C}_1(k_\mathrm{o}\sigma_r r)\exp(\mathrm{i}k_\mathrm{o}\sigma_z z)\hat{\boldsymbol{\phi}}$, *(Equation 4.16a)*

$Z_\mathrm{o}\boldsymbol{H}_0(r,\phi,z) = [-(\mathrm{i}\sigma_z/\sigma_r)\mathcal{C}_1(k_\mathrm{o}\sigma_r r)\hat{\boldsymbol{r}} + \mathcal{C}_0(k_\mathrm{o}\sigma_r r)\hat{\boldsymbol{z}}]\exp(\mathrm{i}k_\mathrm{o}\sigma_z z)$. *(Equation 4.16b)*

TM ($m=0$):

$\boldsymbol{E}_0(r,\phi,z) = [-(\mathrm{i}\sigma_z/\sigma_r)\mathcal{C}_1(k_\mathrm{o}\sigma_r r)\hat{\boldsymbol{r}} + \mathcal{C}_0(k_\mathrm{o}\sigma_r r)\hat{\boldsymbol{z}}]\exp(\mathrm{i}k_\mathrm{o}\sigma_z z)$, *(Equation 4.17a)*

$Z_\mathrm{o}\boldsymbol{H}_0(r,\phi,z) = -(\mathrm{i}\varepsilon/\sigma_r)\mathcal{C}_1(k_\mathrm{o}\sigma_r r)\exp(\mathrm{i}k_\mathrm{o}\sigma_z z)\hat{\boldsymbol{\phi}}$. *(Equation 4.17b)*

In general, the field components in the xy-plane, $\boldsymbol{E}_{m\|}$ and $\boldsymbol{H}_{m\|}$, may be expressed in terms of a superposition of right- and left-circularly polarized states, as follows:

TE: $\boldsymbol{E}_{m\|}(r,\phi,z) = -(\mu/2\sigma_r)\{\mathcal{C}_{m-1}(k_\mathrm{o}\sigma_r r)\exp[\mathrm{i}(m-1)\phi](\hat{\boldsymbol{x}}+\mathrm{i}\hat{\boldsymbol{y}}) + \mathcal{C}_{m+1}(k_\mathrm{o}\sigma_r r)\exp[\mathrm{i}(m+1)\phi](\hat{\boldsymbol{x}}-\mathrm{i}\hat{\boldsymbol{y}})\}$
$\times\exp(\mathrm{i}k_\mathrm{o}\sigma_z z)$,

(Equation 4.18a)

$Z_\mathrm{o}\boldsymbol{H}_m(r,\phi,z) = \{(\mathrm{i}\sigma_z/2\sigma_r)[\mathcal{C}_{m-1}(k_\mathrm{o}\sigma_r r)\exp[\mathrm{i}(m-1)\phi](\hat{\boldsymbol{x}}+\mathrm{i}\hat{\boldsymbol{y}}) - \mathcal{C}_{m+1}(k_\mathrm{o}\sigma_r r)\exp[\mathrm{i}(m+1)\phi](\hat{\boldsymbol{x}}-\mathrm{i}\hat{\boldsymbol{y}})]$
$+ \mathcal{C}_m(k_\mathrm{o}\sigma_r r)\exp(\mathrm{i}m\phi)\hat{\boldsymbol{z}}\}\exp(\mathrm{i}k_\mathrm{o}\sigma_z z)$. *(Equation 4.18b)*

TM: $\boldsymbol{E}_m(r,\phi,z) = \{(\mathrm{i}\sigma_z/2\sigma_r)[\mathcal{C}_{m-1}(k_\mathrm{o}\sigma_r r)\exp[\mathrm{i}(m-1)\phi](\hat{\boldsymbol{x}}+\mathrm{i}\hat{\boldsymbol{y}}) - \mathcal{C}_{m+1}(k_\mathrm{o}\sigma_r r)\exp[\mathrm{i}(m+1)\phi](\hat{\boldsymbol{x}}-\mathrm{i}\hat{\boldsymbol{y}})]$
$+ \mathcal{C}_m(k_\mathrm{o}\sigma_r r)\exp(\mathrm{i}m\phi)\hat{\boldsymbol{z}}\}\exp(\mathrm{i}k_\mathrm{o}\sigma_z z)$, *(Equation 4.19a)*

$Z_\mathrm{o}\boldsymbol{H}_{m\|}(r,\phi,z) = (\varepsilon/2\sigma_r)\{\mathcal{C}_{m-1}(k_\mathrm{o}\sigma_r r)\exp[\mathrm{i}(m-1)\phi](\hat{\boldsymbol{x}}+\mathrm{i}\hat{\boldsymbol{y}}) + \mathcal{C}_{m+1}(k_\mathrm{o}\sigma_r r)\exp[\mathrm{i}(m+1)\phi](\hat{\boldsymbol{x}}-\mathrm{i}\hat{\boldsymbol{y}})\}$
$\times\exp(\mathrm{i}k_\mathrm{o}\sigma_z z)$. *(Equation 4.19b)*

When the region of interest includes the z-axis, the only acceptable cylinder function in the above equations will be $\mathcal{C}_m(\rho) = J_m(\rho)$; this is because $Y_m(\rho)\to\infty$ as $\rho\to 0$. However, if the region of interest excludes the z-axis, the cylinder function will be a superposition of $\mathcal{H}_m^{(1)}(\rho) = J_m(\rho) + \mathrm{i}Y_m(\rho)$, which is an outgoing wave (i.e., one that propagates away from the cylinder axis), and $\mathcal{H}_m^{(2)}(\rho) = J_m(\rho) - \mathrm{i}Y_m(\rho)$, which is an incoming wave.

Bessel function $J_m(\cdot)$ as a superposition of plane-waves

Consider the following p-polarized (TM) plane-wave within a homogeneous, isotropic medium specified by its (ε, μ) parameters:

$\boldsymbol{E}(r,\phi,z,t) = (E_x\hat{\boldsymbol{x}} + E_y\hat{\boldsymbol{y}} + E_z\hat{\boldsymbol{z}})\exp[\mathrm{i}k_\mathrm{o}(\sigma_x x + \sigma_y y + \sigma_z z)]\exp(-\mathrm{i}\omega t)$, *(Equation 4.20a)*

$\boldsymbol{H}(r,\phi,z,t) = (H_x\hat{\boldsymbol{x}} + H_y\hat{\boldsymbol{y}})\exp[\mathrm{i}k_\mathrm{o}(\sigma_x x + \sigma_y y + \sigma_z z)]\exp(-\mathrm{i}\omega t)$. *(Equation 4.20b)*

The authors would like to acknowledge support from the National Science Foundation through CIAN NSF ERC under grant #EEC-0812072.

Here $(x,y) = r(\cos\phi\,\hat{\boldsymbol{x}} + \sin\phi\,\hat{\boldsymbol{y}})$, and $\boldsymbol{\sigma}_r = \sigma_x\hat{\boldsymbol{x}} + \sigma_y\hat{\boldsymbol{y}} = (\sigma'_x + \mathrm{i}\sigma''_x)\hat{\boldsymbol{x}} + (\sigma'_y + \mathrm{i}\sigma''_y)\hat{\boldsymbol{y}} = (\sigma'_x\hat{\boldsymbol{x}} + \sigma'_y\hat{\boldsymbol{y}}) + \mathrm{i}(\sigma''_x\hat{\boldsymbol{x}} + \sigma''_y\hat{\boldsymbol{y}}) = \boldsymbol{\sigma}'_r + \mathrm{i}\boldsymbol{\sigma}''_r$. If $\boldsymbol{\sigma}'_r$ and $\boldsymbol{\sigma}''_r$ happen to be oriented in the same direction within the *xy*-plane, say, at an angle θ relative to the *x*-axis, then $\boldsymbol{\sigma}_r = (\sigma'_r + \mathrm{i}\sigma''_r)(\cos\theta\,\hat{\boldsymbol{x}} + \sin\theta\,\hat{\boldsymbol{y}})$. Maxwell's equations then demand that $\sigma_r^2 + \sigma_z^2 = \mu\varepsilon$; moreover, the field amplitudes must be related as follows:

$$\boldsymbol{E}(r,\phi,z,t) = [-(\sigma_z/\sigma_r)(\cos\theta\,\hat{\boldsymbol{x}} + \sin\theta\,\hat{\boldsymbol{y}}) + \hat{\boldsymbol{z}}]\exp\{\mathrm{i}k_o[\sigma_r r\cos(\theta-\phi) + \sigma_z z - ct]\},$$

(Equation 4.21a)

$$\boldsymbol{H}(r,\phi,z,t) = (\varepsilon/Z_o\sigma_r)(\sin\theta\,\hat{\boldsymbol{x}} - \cos\theta\,\hat{\boldsymbol{y}})\exp\{\mathrm{i}k_o[\sigma_r r\cos(\theta-\phi) + \sigma_z z - ct]\}.$$

(Equation 4.21b)

In these equations the field amplitudes have been normalized to yield a magnitude of unity for E_z. Next, we fix σ_z and σ_r, and consider a superposition of all such plane-waves covering the range of angles θ from 0 to 2π. For the amplitude distribution of these plane-waves we choose $f(\theta) = (2\pi\mathrm{i}^m)^{-1}\exp(\mathrm{i}m\theta)$, with m being an arbitrary integer. The *z*-component of the resulting *E*-field will then be

$$\begin{aligned} E_z(r,\phi) &= (2\pi\mathrm{i}^m)^{-1}\int_0^{2\pi}\exp(\mathrm{i}m\theta)\exp[\mathrm{i}k_o\sigma_r r\cos(\theta-\phi)]\,\mathrm{d}\theta \\ &= (2\pi)^{-1}\exp(\mathrm{i}m\phi)\int_0^{2\pi}\exp(\mathrm{i}m\theta' - \mathrm{i}k_o\sigma_r r\sin\theta')\,\mathrm{d}\theta' \\ &= (2\pi)^{-1}\Big[\int_0^{\pi}\exp(\mathrm{i}m\theta' - \mathrm{i}k_o\sigma_r r\sin\theta')\,\mathrm{d}\theta' + \int_{\pi}^{2\pi}\exp(\mathrm{i}m\theta' - \mathrm{i}k_o\sigma_r r\sin\theta')\,\mathrm{d}\theta'\Big]\exp(\mathrm{i}m\phi). \end{aligned}$$

(Equation 4.22)

A change of variable from θ' to $2\pi-\theta$ reveals the second integral to be the complex conjugate of the first; we thus have

$$E_z(r,\phi) = [(1/\pi)\int_0^{\pi}\cos(m\theta - k_o\sigma_r r\sin\theta)\,\mathrm{d}\theta]\exp(\mathrm{i}m\phi) = J_m(k_o\sigma_r r)\exp(\mathrm{i}m\phi).$$

(Equation 4.23a)

For the component of the *E*-field in the *xy*-plane we then have

$$\begin{aligned} \boldsymbol{E}_{\|}(r,\phi) &= -(\sigma_z/\sigma_r)(2\pi\mathrm{i}^m)^{-1}\int_0^{2\pi}\exp(\mathrm{i}m\theta)(\cos\theta\,\hat{\boldsymbol{x}} + \sin\theta\,\hat{\boldsymbol{y}})\exp[\mathrm{i}k_o\sigma_r r\cos(\theta-\phi)]\,\mathrm{d}\theta \\ &= -(\sigma_z/2\sigma_r)(2\pi\mathrm{i}^m)^{-1}\int\{\exp[\mathrm{i}(m-1)\theta](\hat{\boldsymbol{x}} + \mathrm{i}\hat{\boldsymbol{y}}) + \exp[\mathrm{i}(m+1)\theta](\hat{\boldsymbol{x}} - \mathrm{i}\hat{\boldsymbol{y}})\}\exp[\mathrm{i}k_o\sigma_r r\cos(\theta-\phi)]\,\mathrm{d}\theta \\ &= (\mathrm{i}\sigma_z/2\sigma_r)\{J_{m-1}(k_o\sigma_r r)\exp[\mathrm{i}(m-1)\phi](\hat{\boldsymbol{x}} + \mathrm{i}\hat{\boldsymbol{y}}) - J_{m+1}(k_o\sigma_r r)\exp[\mathrm{i}(m+1)\phi](\hat{\boldsymbol{x}} - \mathrm{i}\hat{\boldsymbol{y}})\}. \end{aligned}$$

(Equation 4.23b)

The above expressions for the various *E*-field components are in agreement with ***(Equation 4.19a)***, corresponding to a TM-polarized cylindrical wave. The corresponding expression for the *H*-field may be similarly derived from ***(Equation 4.21b)***. Derivation of the expressions for a TE-polarized cylindrical wave is straightforward.

The authors would like to acknowledge support from the National Science Foundation through CIAN NSF ERC under grant #EEC-0812072.

Hankel functions $\mathcal{H}_m^{(1,2)}(\rho)$ as superpositions of plane-waves

In general, for a plane-wave such as that described by ***(Equation 4.20)***, the radial propagation constant may be written as $\boldsymbol{\sigma}_r = (\sigma_r' + \mathrm{i}\sigma_r'')(\cos\theta\,\hat{\boldsymbol{x}} + \sin\theta\,\hat{\boldsymbol{y}})$, where $\sigma_r = \sqrt{\boldsymbol{\sigma}_r \cdot \boldsymbol{\sigma}_r} = \sigma_r' + \mathrm{i}\sigma_r''$ $= \sqrt{\mu\varepsilon - \sigma_z^2}$ is the (complex) length of the vector $\boldsymbol{\sigma}_r$. Thus far we have considered only real-valued angles θ, but θ can be complex-valued as well. For example, Fig. 1 shows a path in the complex θ-plane that, starting from $-\frac{1}{2}\pi + \mathrm{i}\infty$, goes down along a vertical leg to the real axis, covers the range $(-\frac{1}{2}\pi, \frac{1}{2}\pi)$ on this axis, then descends along a second vertical leg to $\frac{1}{2}\pi - \mathrm{i}\infty$. (The *complex magnitude* of the vector $\boldsymbol{\sigma}_r$ does not vary as θ traces an arbitrary trajectory in the complex θ-plane, because $\sin^2\theta + \cos^2\theta$ is always equal to unity, irrespective of whether θ is real or complex.)

Since $\boldsymbol{\sigma}_r = \sigma_x\hat{\boldsymbol{x}} + \sigma_y\hat{\boldsymbol{y}} = (\sigma_x'\hat{\boldsymbol{x}} + \sigma_y'\hat{\boldsymbol{y}}) + \mathrm{i}(\sigma_x''\hat{\boldsymbol{x}} + \sigma_y''\hat{\boldsymbol{y}})$, it is clear that $\mathrm{Real}(\boldsymbol{\sigma}_r) = \sigma_x'\hat{\boldsymbol{x}} + \sigma_y'\hat{\boldsymbol{y}}$, a real-valued vector in the xy-plane, defines the direction of phase propagation, whereas $\mathrm{Imag}(\boldsymbol{\sigma}_r) = \sigma_x''\hat{\boldsymbol{x}} + \sigma_y''\hat{\boldsymbol{y}}$, another real-valued vector in the xy-plane, specifies the direction of attenuation. The Hankel function $\mathcal{H}_m^{(1)}$ is obtained from a superposition of the plane-waves located on a trajectory such as T_1 of Figure 4.1(a), when the complex-amplitude distribution for these plane-waves is $(\pi\mathrm{i}^m)^{-1}\exp(\mathrm{i}m\theta)$. In other words,

$$\mathcal{H}_m^{(1)}(k_o\sigma_r r)\exp(\mathrm{i}m\phi) = (\pi\mathrm{i}^m)^{-1}\int_{T_1}\exp(\mathrm{i}m\theta)\exp[\mathrm{i}k_o\sigma_r r\cos(\theta-\phi)]\,\mathrm{d}\theta. \qquad \textit{(Equation 4.24)}$$

A horizontal shift of T_1 by ϕ does not alter the value of the above integral, provided that $-\frac{1}{2}\pi < \phi < \frac{1}{2}\pi$, which is needed to ensure that the integrand goes to zero at the initial and final points of T_1. In fact, any deformation of T_1 will not affect the resulting integral, so long as the trajectory's start and finish points remain within $(-\pi, 0) + \mathrm{i}\infty$ and $(0, \pi) - \mathrm{i}\infty$, respectively. We conclude that

$$\mathcal{H}_m^{(1)}(k_o\sigma_r r) = (\pi\mathrm{i}^m)^{-1}\int_{T_1}\exp(\mathrm{i}m\theta)\exp(\mathrm{i}k_o\sigma_r r\cos\theta)\,\mathrm{d}\theta. \qquad \textit{(Equation 4.25)}$$

Therefore, in the region $x > 0$ of the xy-plane, where $-\frac{1}{2}\pi < \phi < \frac{1}{2}\pi$, ***(Equation 4.25)*** describes $\mathcal{H}_m^{(1)}(k_o\sigma_r r)$ as a superposition of outgoing plane-waves. Similar considerations apply to $\mathcal{H}_m^{(2)}(k_o\sigma_r r)$ with the exception that the θ-plane trajectory in this case is T_2 of ***Figure 4.1(b)***. The plane-waves that constitute type 2 Hankel functions are thus seen to be plane-waves that propagate toward the center of the coordinate system.

For a generalized plane-wave, given the z-component $k_o\sigma_z$ of the propagation vector, the radial phase-factor may be written as follows:

$$\mathrm{i}k_o\boldsymbol{\sigma}_r\cdot\boldsymbol{r} = \mathrm{i}k_o(\sigma_r' + \mathrm{i}\sigma_r'')(\cos\theta\,\hat{x} + \sin\theta\,\hat{y})\cdot r(\cos\phi\,\hat{x} + \sin\phi\,\hat{y}) = \mathrm{i}k_o r(\sigma_r' + \mathrm{i}\sigma_r'')\cos(\theta' + \mathrm{i}\theta'' - \phi)$$
$$= -k_o r[\sigma_r''\cos(\theta'-\phi)\,\mathrm{ch}\,\theta'' - \sigma_r'\sin(\theta'-\phi)\,\mathrm{sh}\,\theta''] + \mathrm{i}k_o r[\sigma_r'\cos(\theta'-\phi)\,\mathrm{ch}\,\theta'' + \sigma_r''\sin(\theta'-\phi)\,\mathrm{sh}\,\theta''].$$

(Equation 4.26)

The authors would like to acknowledge support from the National Science Foundation through CIAN NSF ERC under grant #EEC-0812072.

When $\theta'' \to +\infty$, $\mathrm{sh}\,\theta''$ and $\mathrm{ch}\,\theta''$ approach each other on their way to $+\infty$; it is thus required for the real part of the above expression to be negative, that is, $\sigma_r'' \cos(\theta' - \phi) - \sigma_r' \sin(\theta' - \phi) > 0$. When $\theta'' \to -\infty$, however, we must have $\sigma_r'' \cos(\theta' - \phi) + \sigma_r' \sin(\theta' - \phi) > 0$. Let us define the real-valued angle $\theta_0 = \tan^{-1}(\sigma_r''/\sigma_r')$; clearly, since $\sigma_r'' \geq 0$, we have $0 \leq \theta_0 \leq \frac{1}{2}\pi$ when $\sigma_r' \geq 0$, and $-\frac{1}{2}\pi \leq \theta_0 \leq 0$ when $\sigma_r' \leq 0$. The starting point of the trajectory must, therefore, lie in the region $(\theta_0 - \pi, \theta_0) + \mathrm{i}\infty$ when $\theta_0 \geq 0$ and in $(\theta_0, \theta_0 + \pi) + \mathrm{i}\infty$ when $\theta_0 \leq 0$. Similarly, the trajectory's terminal point must be in $(-\theta_0, \pi - \theta_0) - \mathrm{i}\infty$ when $\theta_0 \geq 0$, and in $(-\pi - \theta_0, -\theta_0) - \mathrm{i}\infty$ when $\theta_0 \leq 0$; see ***Figure 4.2***.

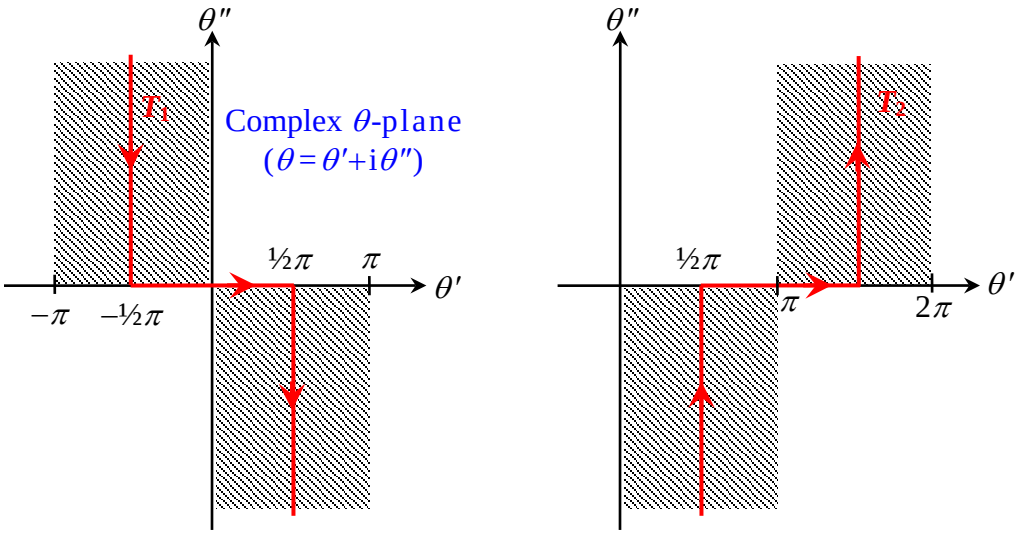

Figure 4.1 (a) Trajectory T_1 in the complex θ-plane for type 1 Hankel function $\mathscr{H}_m^{(1)}(\rho)$. (b) Trajectory T_2 for type 2 Hankel function $\mathscr{H}_m^{(2)}(\rho)$. Any deformation of these trajectories is allowed, so long as the start and finish points remain in the corresponding shaded regions. Note that either trajectory may be translated horizontally by an amount ϕ, where $-\frac{1}{2}\pi < \phi < \frac{1}{2}\pi$, without affecting the resultant integral.

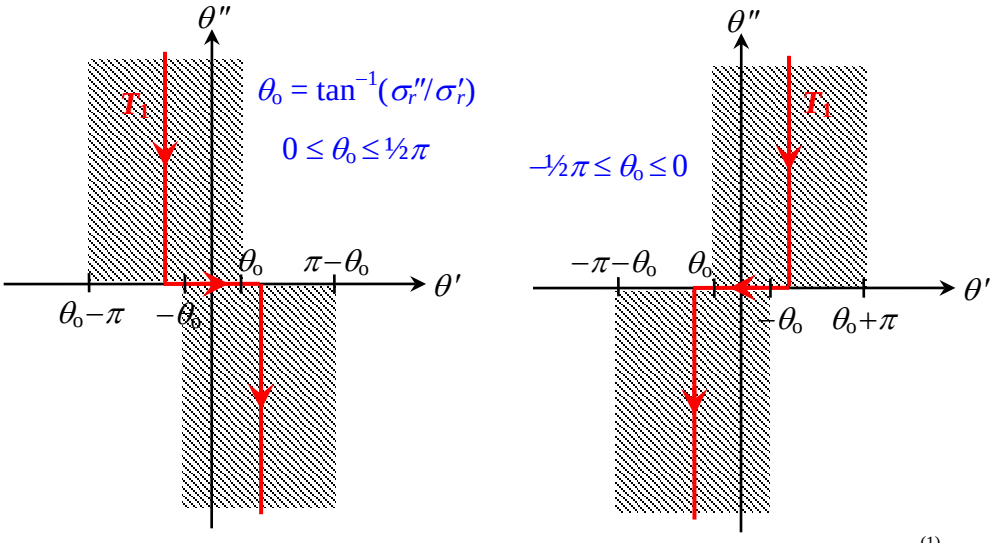

Figure 4.2. Trajectory T_1 in the complex θ-plane for the defining integral of $\mathscr{H}_m^{(1)}(\rho)$ in the general case when $\sigma_r = \sigma_r' + \mathrm{i}\sigma_r''$. In general $\sigma_r'' \geq 0$. In (a) $\sigma_r' \geq 0$, whereas in (b) $\sigma_r' \leq 0$.

The authors would like to acknowledge support from the National Science Foundation through CIAN NSF ERC under grant #EEC-0812072.

Figure 4.3 shows, for a given value of $\sigma_r = \sigma_r' + \mathrm{i}\sigma_r''$, the trajectories of Real(σ_r) and Imag(σ_r), corresponding to the θ-trajectory T_1 depicted in **Figure 4.2(a)**. While the phase-fronts of different plane-waves could propagate in various directions, their amplitudes essentially decay along the horizontal axis. Within the $x > 0$ half-space, the superposition of all these plane-waves produces, in accordance with **Equation (4.24)**, the function $\mathscr{H}_m^{(1)}(k_o\sigma_r r)\exp(\mathrm{i}m\phi)\exp(\mathrm{i}k_o\sigma_z z)$. Note that, since θ is real-valued on the circular sections of the trajectories, Real(σ_r) and Imag(σ_r) are parallel to each other on the circular trajectories. In contrast, on the vertical legs of T_1, the trajectories of Real(σ_r) and Imag(σ_r) are nearly orthogonal to each other.

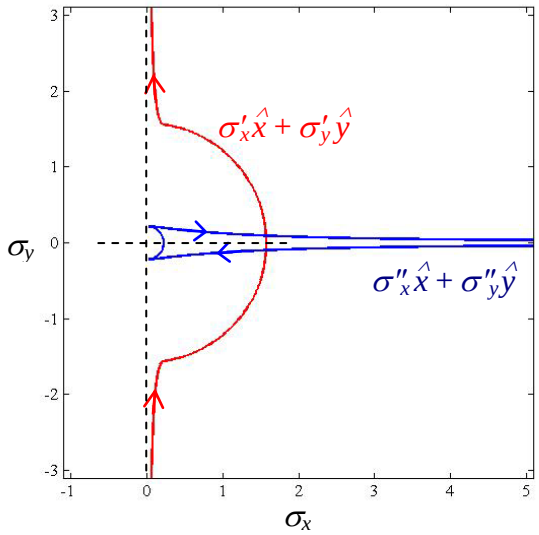

Figure 4.3. $\sigma_x\sigma_y$-plane trajectories of Real(σ_r) (red) and Imag(σ_r) (blue) for the case of $\mu\varepsilon = 2.5 + 0.7\mathrm{i}$ and $\sigma_z = 0.25$, corresponding to $\sigma_r = 1.577 + 0.222\mathrm{i}$ and $\theta_o \approx 8°$. The θ-plane integration path is depicted in Figure 4.2(a).

4.2 Guided modes and surface-plasmon-polaritons in systems of cylindrical symmetry

The analysis presented in this section is applicable whenever the medium hosting the electromagnetic wave consists of two regions: inside a cylinder of radius r_o the material parameters are (ε_1, μ_1), while outside the cylinder, the parameters are (ε_2, μ_2). Examples include step-index optical fibers supporting guided modes, and metallic nano-wires or nano-rods (with or without a dielectric coating) that host surface-plasmon-polariton excited waves.

In general, a superposition of TE and TM waves in both regions (i.e., inside and outside the cylinder of radius r_o) is needed to satisfy the continuity of E_z, H_z, E_ϕ, H_ϕ at the $r = r_o$ boundary. Inside the cylinder, the appropriate cylinder function is $J_m(k_o\sigma_{r1}r)$, and the (initially unknown) coefficients for TM and TE modes are A_1 and B_1, respectively. Outside the cylinder, the appropriate function is $\mathscr{H}_m^{(1)}(k_o\sigma_{r2}r)$, while the corresponding coefficients are A_2 and B_2. The continuity equations are thus written

The authors would like to acknowledge support from the National Science Foundation through CIAN NSF ERC under grant #EEC-0812072.

Continuity of E_z: $A_1 J_m(k_o\sigma_{r1}r_o) = A_2\mathscr{H}_m^{(1)}(k_o\sigma_{r2}r_o)$,

(Equation 4.27a)

Continuity of H_z: $B_1 J_m(k_o\sigma_{r1}r_o) = B_2\mathscr{H}_m^{(1)}(k_o\sigma_{r2}r_o)$,

(Equation 4.27b)

Continuity of E_ϕ: $A_1(m\sigma_z/k_o r_o\sigma_{r1}^2)\,J_m(k_o\sigma_{r1}r_o) + B_1(\mathrm{i}\mu_1/\sigma_{r1})\,J_m'(k_o\sigma_{r1}r_o) =$

$A_2(m\sigma_z/k_o r_o\sigma_{r2}^2)\,\mathscr{H}_m^{(1)}(k_o\sigma_{r2}r_o) + B_2(\mathrm{i}\mu_2/\sigma_{r2})\,\mathscr{H}_m'^{(1)}(k_o\sigma_{r2}r_o)$,

(Equation 4.27c)

Continuity of H_ϕ: $A_1(\mathrm{i}\varepsilon_1/\sigma_{r1})\,J_m'(k_o\sigma_{r1}r_o) - B_1(m\sigma_z/k_o r_o\sigma_{r1}^2)\,J_m(k_o\sigma_{r1}r_o) =$

$A_2(\mathrm{i}\varepsilon_2/\sigma_{r2})\,\mathscr{H}_m'^{(1)}(k_o\sigma_{r2}r_o) - B_2(m\sigma_z/k_o r_o\sigma_{r2}^2)\,\mathscr{H}_m^{(1)}(k_o\sigma_{r2}r_o)$.

(Equation 4.27d)

The continuity of $D_r = \varepsilon_o\varepsilon E_r$ is guaranteed by the continuity of H_z and H_ϕ; similarly, the continuity of $B_r = \mu_o\mu H_r$ is guaranteed by the continuity of E_z and E_ϕ. The above equations can be solved for A_1, B_1, A_2, B_2 provided that the following characteristic equation is satisfied:

$$\left[\frac{\mu_1}{\sqrt{\mu_1\varepsilon_1-\sigma_z^2}}\frac{J_m'(k_o\sigma_{r1}r_o)}{J_m(k_o\sigma_{r1}r_o)} - \frac{\mu_2}{\sqrt{\mu_2\varepsilon_2-\sigma_z^2}}\frac{\mathscr{H}_m'^{(1)}(k_o\sigma_{r2}r_o)}{\mathscr{H}_m^{(1)}(k_o\sigma_{r2}r_o)}\right]\times$$

$$\left[\frac{\varepsilon_1}{\sqrt{\mu_1\varepsilon_1-\sigma_z^2}}\frac{J_m'(k_o\sigma_{r1}r_o)}{J_m(k_o\sigma_{r1}r_o)} - \frac{\varepsilon_2}{\sqrt{\mu_2\varepsilon_2-\sigma_z^2}}\frac{\mathscr{H}_m'^{(1)}(k_o\sigma_{r2}r_o)}{\mathscr{H}_m^{(1)}(k_o\sigma_{r2}r_o)}\right] = \frac{m^2\sigma_z^2}{k_o^2 r_o^2}\left(\frac{1}{\mu_1\varepsilon_1-\sigma_z^2} - \frac{1}{\mu_2\varepsilon_2-\sigma_z^2}\right)^2. \quad \textit{(Equation 4.28)}$$

Given the values of $m, k_o, r_o, \mu_1, \varepsilon_1, \mu_2, \varepsilon_2$, one may solve **(Equation 4.28)** numerically for acceptable values of σ_z. In lossless media (i.e., real-valued μ_1, ε_1, μ_2, ε_2), if a real-valued σ_z is found, it will correspond to a guided mode (e.g., in glass fibers, where $\sqrt{\mu_2\varepsilon_2} < \sigma_z < \sqrt{\mu_1\varepsilon_1}$). In general, however, σ_z will be complex, corresponding to an attenuated mode along the z-axis.

A special case would arise when $\sigma_z = 0$; here TE and TM modes are decoupled, and the characteristic equation for each may be written independently of the other, as follows:

TE: $$\sqrt{\mu_1/\varepsilon_1}\,\frac{J_m'(k_o\sqrt{\mu_1\varepsilon_1}\,r_o)}{J_m(k_o\sqrt{\mu_1\varepsilon_1}\,r_o)} = \sqrt{\mu_2/\varepsilon_2}\,\frac{\mathscr{H}_m'^{(1)}(k_o\sqrt{\mu_2\varepsilon_2}\,r_o)}{\mathscr{H}_m^{(1)}(k_o\sqrt{\mu_2\varepsilon_2}\,r_o)}. \quad \textit{(Equation 4.29)}$$

TM: $$\sqrt{\varepsilon_1/\mu_1}\,\frac{J_m'(k_o\sqrt{\mu_1\varepsilon_1}\,r_o)}{J_m(k_o\sqrt{\mu_1\varepsilon_1}\,r_o)} = \sqrt{\varepsilon_2/\mu_2}\,\frac{\mathscr{H}_m'^{(1)}(k_o\sqrt{\mu_2\varepsilon_2}\,r_o)}{\mathscr{H}_m^{(1)}(k_o\sqrt{\mu_2\varepsilon_2}\,r_o)}. \quad \textit{(Equation 4.30)}$$

This case probably never arises in practice, because either *(Equation 4.29)* or *(Equation 4.30)* can be satisfied only by coincidence, when the cylinder radius r_o happens to be just right for the two media inside and outside the cylinder. Even then it is hard to see how energy can be conserved,

The authors would like to acknowledge support from the National Science Foundation through CIAN NSF ERC under grant #EEC-0812072.

because the entire wave is a standing wave in cylindrical coordinates. One should investigate the properties of the Poynting vector in order to gain further insight into this type of problem.

Another special case is when $m = 0$; here once again TE and TM modes are decoupled, and the characteristic equation for each mode becomes:

TE:
$$\frac{\mu_1}{\sqrt{\mu_1\varepsilon_1-\sigma_z^2}}\frac{J_1(k_o\sqrt{\mu_1\varepsilon_1-\sigma_z^2}\,r_o)}{J_0(k_o\sqrt{\mu_1\varepsilon_1-\sigma_z^2}\,r_o)}=\frac{\mu_2}{\sqrt{\mu_2\varepsilon_2-\sigma_z^2}}\frac{\mathcal{H}_1^{(1)}(k_o\sqrt{\mu_2\varepsilon_2-\sigma_z^2}\,r_o)}{\mathcal{H}_0^{(1)}(k_o\sqrt{\mu_2\varepsilon_2-\sigma_z^2}\,r_o)}.$$

(Equation 4.31)

TM:
$$\frac{\varepsilon_1}{\sqrt{\mu_1\varepsilon_1-\sigma_z^2}}\frac{J_1(k_o\sqrt{\mu_1\varepsilon_1-\sigma_z^2}\,r_o)}{J_0(k_o\sqrt{\mu_1\varepsilon_1-\sigma_z^2}\,r_o)}=\frac{\varepsilon_2}{\sqrt{\mu_2\varepsilon_2-\sigma_z^2}}\frac{\mathcal{H}_1^{(1)}(k_o\sqrt{\mu_2\varepsilon_2-\sigma_z^2}\,r_o)}{\mathcal{H}_0^{(1)}(k_o\sqrt{\mu_2\varepsilon_2-\sigma_z^2}\,r_o)}.$$

(Equation 4.32)

As before, given the values of k_o, r_o, μ_1, ε_1, μ_2, ε_2, one can solve ***(Equation 4.31) or (Equation 4.32)*** numerically to determine the acceptable values of σ_z.

The authors would like to acknowledge support from the National Science Foundation through CIAN NSF ERC under grant #EEC-0812072.

4.3 Energy flux and the Poynting vector

For the TE and TM modes described by *(Equation 4.14)* and *(Equation 4.15)*, the time-averaged Poynting vector $\langle \boldsymbol{S} \rangle = \tfrac{1}{2}\mathrm{Real}(\boldsymbol{E} \times \boldsymbol{H}^*)$ is given by

TE:

$$\langle S_r \rangle = \frac{\exp[-2k_o \mathrm{Im}(\sigma_z) z]}{2Z_o |\mu\varepsilon - \sigma_z^2|} \left\{ \mathrm{Im}[\mu^* \sigma_r \mathscr{C}_m(k_o \sigma_r r) \mathscr{C}^*_{m+1}(k_o \sigma_r r)] - \frac{m\,\mathrm{Im}(\mu^* \sigma_r^2)}{k_o r |\mu\varepsilon - \sigma_z^2|} |\mathscr{C}_m(k_o \sigma_r r)|^2 \right\},$$

(Equation 4.33a)

$$\langle S_\phi \rangle = \frac{m\,\mathrm{Re}[\mu/(\mu\varepsilon - \sigma_z^2)] \exp[-2k_o \mathrm{Im}(\sigma_z) z]}{2Z_o k_o r} |\mathscr{C}_m(k_o \sigma_r r)|^2,$$

(Equation 4.33b)

$$\langle S_z \rangle = \frac{\mathrm{Re}(\mu^* \sigma_z) \exp[-2k_o \mathrm{Im}(\sigma_z) z]}{2Z_o |\mu\varepsilon - \sigma_z^2|} \left\{ |\mathscr{C}'_m(k_o \sigma_r r)|^2 + \frac{m^2}{k_o^2 r^2 |\mu\varepsilon - \sigma_z^2|} |\mathscr{C}_m(k_o \sigma_r r)|^2 \right\}.$$

(Equation 4.33c)

TM:

$$\langle S_r \rangle = \frac{\exp[-2k_o \mathrm{Im}(\sigma_z) z]}{2Z_o |\mu\varepsilon - \sigma_z^2|} \left\{ \mathrm{Im}[\varepsilon^* \sigma_r \mathscr{C}_m(k_o \sigma_r r) \mathscr{C}^*_{m+1}(k_o \sigma_r r)] - \frac{m\,\mathrm{Im}(\varepsilon^* \sigma_r^2)}{k_o r |\mu\varepsilon - \sigma_z^2|} |\mathscr{C}_m(k_o \sigma_r r)|^2 \right\},$$

(Equation 4.34a)

$$\langle S_\phi \rangle = \frac{m\,\mathrm{Re}[\varepsilon/(\mu\varepsilon - \sigma_z^2)] \exp[-2k_o \mathrm{Im}(\sigma_z) z]}{2Z_o k_o r} |\mathscr{C}_m(k_o \sigma_r r)|^2,$$

(Equation 4.34b)

$$\langle S_z \rangle = \frac{\mathrm{Re}(\varepsilon^* \sigma_z) \exp[-2k_o \mathrm{Im}(\sigma_z) z]}{2Z_o |\mu\varepsilon - \sigma_z^2|} \left\{ |\mathscr{C}'_m(k_o \sigma_r r)|^2 + \frac{m^2}{k_o^2 r^2 |\mu\varepsilon - \sigma_z^2|} |\mathscr{C}_m(k_o \sigma_r r)|^2 \right\}.$$

(Equation 4.34c)

When a TE mode of amplitude *A* is superimposed on a TM mode of amplitude *B*, the following cross-terms will appear in the expression of the Poynting vector:

Cross terms:

$$\langle S_r \rangle = \frac{m\,\mathrm{Im}(A^* B)}{Z_o k_o r} \exp[-2k_o \mathrm{Im}(\sigma_z) z]\, \mathrm{Im}[\sigma_z/(\mu\varepsilon - \sigma_z^2)] |\mathscr{C}_m(k_o \sigma_r r)|^2,$$

(Equation 4.35a)

$$\langle S_\phi \rangle = \frac{\mathrm{Im}(A^* B)}{Z_o} \exp[-2k_o \mathrm{Im}(\sigma_z) z]\, \mathrm{Re}[(\sigma_z/\sigma_r) \mathscr{C}^*_m(k_o \sigma_r r) \mathscr{C}'_m(k_o \sigma_r r)],$$

(Equation 4.35b)

$$\langle S_z \rangle = \frac{m\,\mathrm{Im}[A^* B(\mu^* \varepsilon + |\sigma_z|^2)]}{Z_o k_o r |\mu\varepsilon - \sigma_z^2|} \exp[-2k_o \mathrm{Im}(\sigma_z) z]\, \mathrm{Re}[\mathscr{C}_m(k_o \sigma_r r) \mathscr{C}'^*_m(k_o \sigma_r r)/\sigma_r].$$

(Equation 4.35c)

The authors would like to acknowledge support from the National Science Foundation through CIAN NSF ERC under grant #EEC-0812072.

The above equations will be useful when analyzing the behavior of optical fibers, hollow-tube waveguides, nano-wires, nano-rods, and many similar systems of cylindrical symmetry. The analysis of propagating or guided modes in such systems is highly complex and specialized, requiring a textbook of its own. We do hope, however, that the present chapter has provided the reader with the necessary background to facilitate his/her future forays into the subject.

The authors would like to acknowledge support from the National Science Foundation through CIAN NSF ERC under grant #EEC-0812072.

References

1. For an extensive listing of the various properties of Bessel functions see I. S. Gradshteyn and I. M. Ryzhik, *Table of Integrals, Series, and Products*, seventh edition, Academic Press, 2007.
2. For applications of modal analysis to step-index optical fibers see G. Keiser, *Optical Fiber Communications*, 3rd edition, McGraw-Hill, New York, 2000.
3. For applications of modal analysis to cylindrical waveguides see S. Ramo, J. A. Whinnery, and T. Van Duzer, *Fields and Waves in Communications Electronics*, Wiley, New York, 1994.
4. For a discussion of surface-plasmon-polaritons see C. A. Pfeiffer, E. N. Economou, and K. L. Ngai, "*Surface polaritons in a circularly cylindrical interface: Surface plasmons,*" Physical Review B **10**, (1974).

The authors would like to acknowledge support from the National Science Foundation through CIAN NSF ERC under grant #EEC-0812072.

Appendix

Bessel Functions and Their Properties

Bessel functions are solutions of the second-order differential equation

Gradshteyn & Ryzhik 8.401

$$\frac{d^2y(x)}{dx^2}+\frac{1}{x}\frac{dy(x)}{dx}+(1-\frac{\nu^2}{x^2})y(x)=0. \qquad \textit{(Equation 4.A1)}$$

Although the function $y(\cdot)$, the variable x, and the constant parameter ν are generally complex-valued, we shall primarily be interested in cases where $y(\cdot)$, x, and ν are real. For a given value of ν, the 2nd order equation (A1) has two independent solutions: Bessel functions of the *first kind*, $J_\nu(x)$, and Bessel functions of the *second kind*, $Y_\nu(x)$; the latter are sometimes referred to as Neumann functions. Bessel functions of the *third kind*, types 1 and 2, also known as Hankel functions, are constructed from $J_\nu(\cdot)$ and $Y_\nu(\cdot)$ as follows:

$$H_\nu^{(1)}(x)=J_\nu(x)+iY_\nu(x); \qquad \textit{(Equation 4.A2a)}$$

$$H_\nu^{(2)}(x)=J_\nu(x)-iY_\nu(x). \qquad \textit{(Equation 4.A2b)}$$

In what follows, we list some of the important properties of the Bessel functions without attempting to prove them; such proofs may be found in any standard treatise on Bessel functions.

For $\nu=n\geq 0$ (i.e., ν a non-negative integer), the solutions of Eq. (A1) are given by

G&R 8.402

$$J_n(x)=(x/2)^n\sum_{k=0}^{\infty}\frac{(-1)^k\,(x/2)^{2k}}{k!\,(n+k)!} \qquad n=0,1,2,3... \qquad \textit{(Equation 4.A3)}$$

G&R 8.403–2

$$Y_n(x)=\frac{2}{\pi}[c+\ln(x/2)]J_n(x)-\frac{(x/2)^{-n}}{\pi}\sum_{k=0}^{n-1}\frac{(n-k-1)!}{k!}(x/2)^{2k}$$
$$-\frac{(x/2)^n}{\pi(n!)}\sum_{k=1}^{n}\frac{1}{k}\;-\frac{(x/2)^n}{\pi}\sum_{k=1}^{\infty}\frac{(-1)^k\,(x/2)^{2k}}{k!\,(k+n)!}\left[\sum_{m=1}^{n+k}\frac{1}{m}+\sum_{m=1}^{k}\frac{1}{m}\right].$$

(Equation 4.A4)

In the above equations, 0! is defined as 1. Also, when the upper limit of a sum over k is below its lower limit, the term containing the sum must be set to zero; this occurs for $n=0$ in the 2nd and 3rd terms on the right-hand-side of Equation 4.A4, thus reducing the expression for $Y_0(x)$ to one containing the 1st and 4th terms only. Finally, the Euler constant c appearing in *Equation (4.A4)* is defined as

$$c=\lim_{n\to\infty}\left(\sum_{k=1}^{n}\frac{1}{k}-\ln n\right)=0.577215...\cdot \qquad \textit{(Equation 4.A5)}$$

Given below are expanded forms of $J_0(x)$, $Y_0(x)$, $J_1(x)$, and $Y_1(x)$; plots of these functions appear in Fig. A1.

The authors would like to acknowledge support from the National Science Foundation through CIAN NSF ERC under grant #EEC-0812072.

$$J_0(x) = 1 - \frac{(x/2)^2}{(1!)^2} + \frac{(x/2)^4}{(2!)^2} - \frac{(x/2)^6}{(3!)^2} + \cdots, \qquad \textit{(Equation 4.A6)}$$

$$J_1(x) = \frac{1}{2}x - \frac{(x/2)^3}{1!2!} + \frac{(x/2)^5}{2!3!} - \frac{(x/2)^7}{3!4!} + \cdots, \qquad \textit{(Equation 4.A7)}$$

$$Y_0(x) = \frac{2}{\pi}[c + \ln(x/2)]\, J_0(x) + \frac{2}{\pi}\left[\frac{(x/2)^2}{(1!)^2} - (1+\tfrac{1}{2})\frac{(x/2)^4}{(2!)^2} + (1+\tfrac{1}{2}+\tfrac{1}{3})\frac{(x/2)^6}{(3!)^2} - \cdots\right],$$

(Equation 4.A8)

$$Y_1(x) = \frac{2}{\pi}[c + \ln(x/2\ ])J_1(x) - \frac{2}{\pi x} - \frac{x}{2\pi}\left[1 + \sum_{k=1}^{\infty}\frac{(-1)^k\,(x/2)^{2k}}{k!\,(k+1)!}\left(\sum_{m=1}^{k+1}\frac{1}{m} + \sum_{m=1}^{k}\frac{1}{m}\right)\right].$$

(Equation 4.A9)

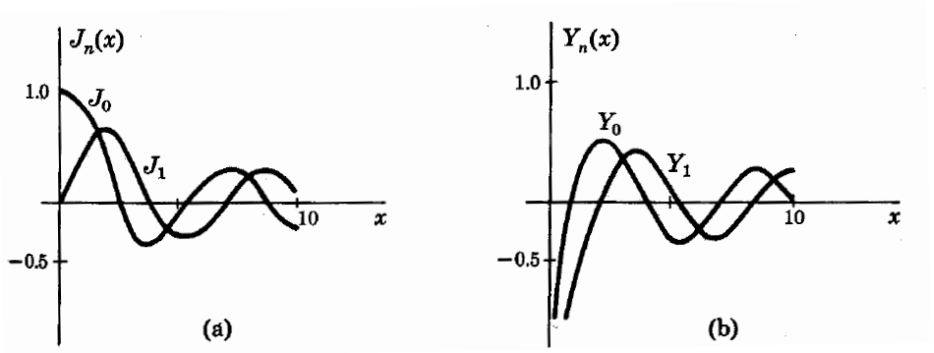

Figure 4.A1. (a) Plots of $J_0(x)$ and $J_1(x)$. (b) Plots of $Y_0(x)$ and $Y_1(x)$.

Changing the sign of a Bessel function's argument modifies the function in the following way:

$$J_n(-x) = (-1)^n J_n(x), \qquad \textit{(Equation 4.A10)}$$

$$Y_n(-x) = (-1)^n [Y_n(x) + 2\mathrm{i}\, J_n(x)]. \qquad \textit{(Equation 4.A11)}$$

When n is fixed and $x \to 0$, the small-argument limiting forms of the Bessel functions are

$$J_n(x) \sim \frac{(x/2)^n}{n!}; \quad n \geq 0, \qquad \textit{(Equation 4.A12)}$$

$$Y_n(x) \sim -\frac{(n-1)!}{\pi}(x/2)^{-n}; \quad n \geq 1, \qquad \textit{(Equation 4.A13)}$$

$$Y_0(x) \sim \frac{2}{\pi}\ln x. \qquad \textit{(Equation 4.A14)}$$

Similarly, when $x \to \infty$, the large-argument limiting forms become

G&R **8.451**–1 $$J_n(x) \to \sqrt{2/(\pi x)}\,\cos[x - (n\pi/2) - (\pi/4)], \qquad \textit{(Equation 4.A15)}$$

G&R **8.451**–2 $$Y_n(x) \to \sqrt{2/(\pi x)}\,\sin[x - (n\pi/2) - (\pi/4)]. \qquad \textit{(Equation 4.A16)}$$

The authors would like to acknowledge support from the National Science Foundation through CIAN NSF ERC under grant #EEC-0812072.

The first-derivatives of the Bessel functions are given by

G&R **8.473**–4
$$J_0'(x) = -J_1(x), \qquad \textit{(Equation 4.A17)}$$

G&R **8.473**–5
$$Y_0'(x) = -Y_1(x), \qquad \textit{(Equation 4.A18)}$$

G&R **8.472**–1,2
$$J_n'(x) = J_{n-1}(x) - (n/x)\,J_n(x) = -J_{n+1}(x) + (n/x)\,J_n(x), \qquad \textit{(Equation 4.A19)}$$

G&R **8.472**–1,2
$$Y_n'(x) = Y_{n-1}(x) - (n/x)\,Y_n(x) = -Y_{n+1}(x) + (n/x)\,Y_n(x). \qquad \textit{(Equation 4.A20)}$$

The modified Bessel functions of imaginary argument are the real-valued functions $I_n(\cdot)$ and $K_n(\cdot)$ defined as follows:

$$I_n(x) = \mathrm{i}^{-n} J_n(\mathrm{i}x), \qquad \text{G\&R } \mathbf{8.406}\text{–3} \qquad \textit{(Equation 4.A21)}$$

$$K_n(x) = \mathrm{i}^{n+1}(\pi/2)\,H_n^{(1)}(\mathrm{i}x). \qquad \text{G\&R } \mathbf{8.407}\text{–1} \qquad \textit{(Equation 4.A22)}$$

Figure 4.A2 shows plots of the functions $I_0(x)$, $I_1(x)$, $K_0(x)$, and $K_1(x)$.

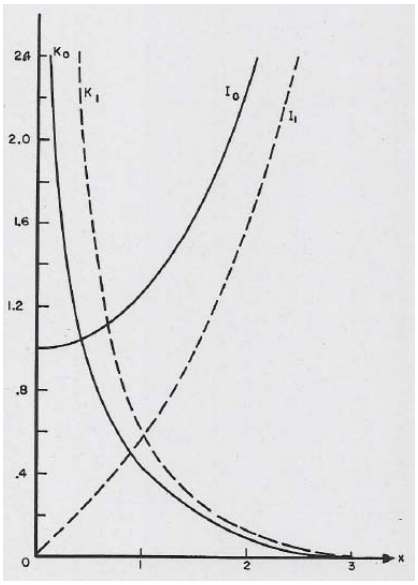

Figure 4.A2. Plots of $I_0(x)$, $I_1(x)$, $K_0(x)$, and $K_1(x)$.

Two useful identities involving Bessel functions of different kinds and different orders are

$$Y_n(x)\,J_{n+1}(x) - J_n(x)\,Y_{n+1}(x) = \frac{2}{\pi x}, \qquad \text{G\&R } \mathbf{8.477}\text{–1} \qquad \textit{(Equation 4.A23)}$$

$$I_n(x)\,K_{n+1}(x) + K_n(x)\,I_{n+1}(x) = \frac{1}{x}. \qquad \text{G\&R } \mathbf{8.477}\text{–2} \qquad \textit{(Equation 4.A24)}$$

Finally, a frequently-encountered integral representation of the Bessel function of the first kind, n^{th} order is given below.

$$\int_0^{\pi} \cos(nx)\exp(\mathrm{i}\beta\cos x)\,\mathrm{d}x = \mathrm{i}^n \pi J_n(\beta). \qquad \text{G\&R } \mathbf{3.915}\text{–2} \qquad \textit{(Equation 4.A25)}$$

The authors would like to acknowledge support from the National Science Foundation through CIAN NSF ERC under grant #EEC-0812072.

For an extensive listing of the various properties of the Bessel functions see I. S. Gradshteyn and I. M. Ryzhik, *Table of Integrals, Series, and Products*, seventh edition, Academic Press, 2007.

The authors would like to acknowledge support from the National Science Foundation through CIAN NSF ERC under grant #EEC-0812072.